Supplementary Information

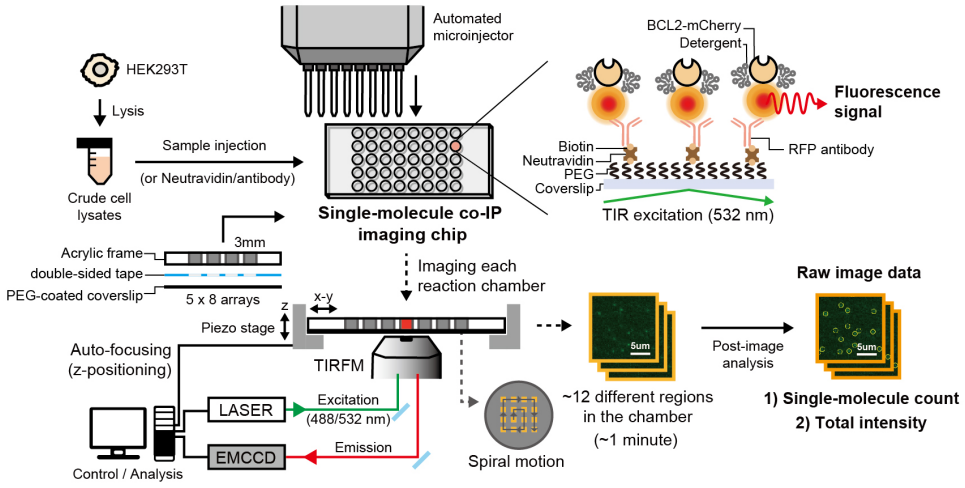

Supplementary Fig. 1: Overview of instrumental setup and analysis strategy of single-molecule co-IP. Schematic of the single-molecule co-IP with TIR fluorescence microscope (TIRFM) setup and co-IP analysis for counting fluorescence signals of immobilized proteins and PPI complexes. The single-molecule co-IP imaging chip was assembled using double-sided tape with an acrylic frame and a PEG-coated coverslip. An automated microinjector was used to inject Neutravidin, antibody, and crude cell lysates into the reaction chamber. After surface-immobilization or PPI reaction, approximately 12 independent images were taken. Target single-molecule fluorescence counts (single-molecule count) and the total intensity data within the field of view (50×100 μm^2) of the raw image data were obtained through computational post-image analysis. The detailed protocol is described in the Method section.

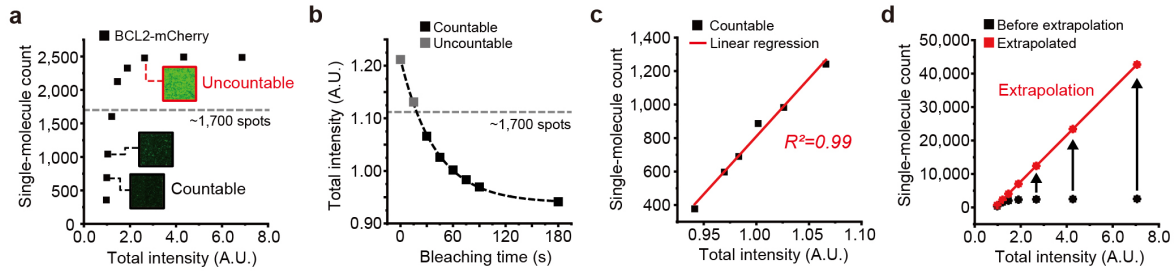

Supplementary Fig. 2: Extrapolation of single-molecule count from the total intensity of uncountable images. a, Single-molecule count dependent on the total intensity of surface-immobilized BCL2-mCherry obtained from the image data without extrapolating the uncountable images. From our current setting, an image containing over 1,700 single-molecule fluorescence spots within a field of view is considered an uncountable image. Single-molecule count of the uncountable image is predicted by fitting the total intensity values to the linear regression equation obtained from the countable images. **b**, Photobleaching kinetics of surface-immobilized mCherry signals from the uncountable image depending on the bleaching time. **c**, The linear correlation between single-molecule count and total intensity of surface-immobilized mCherry from countable images in (c) after photobleaching. **d**, Extrapolation of single-molecule count from the total intensity of uncountable images. The extrapolation formula obtained in (c) was used.

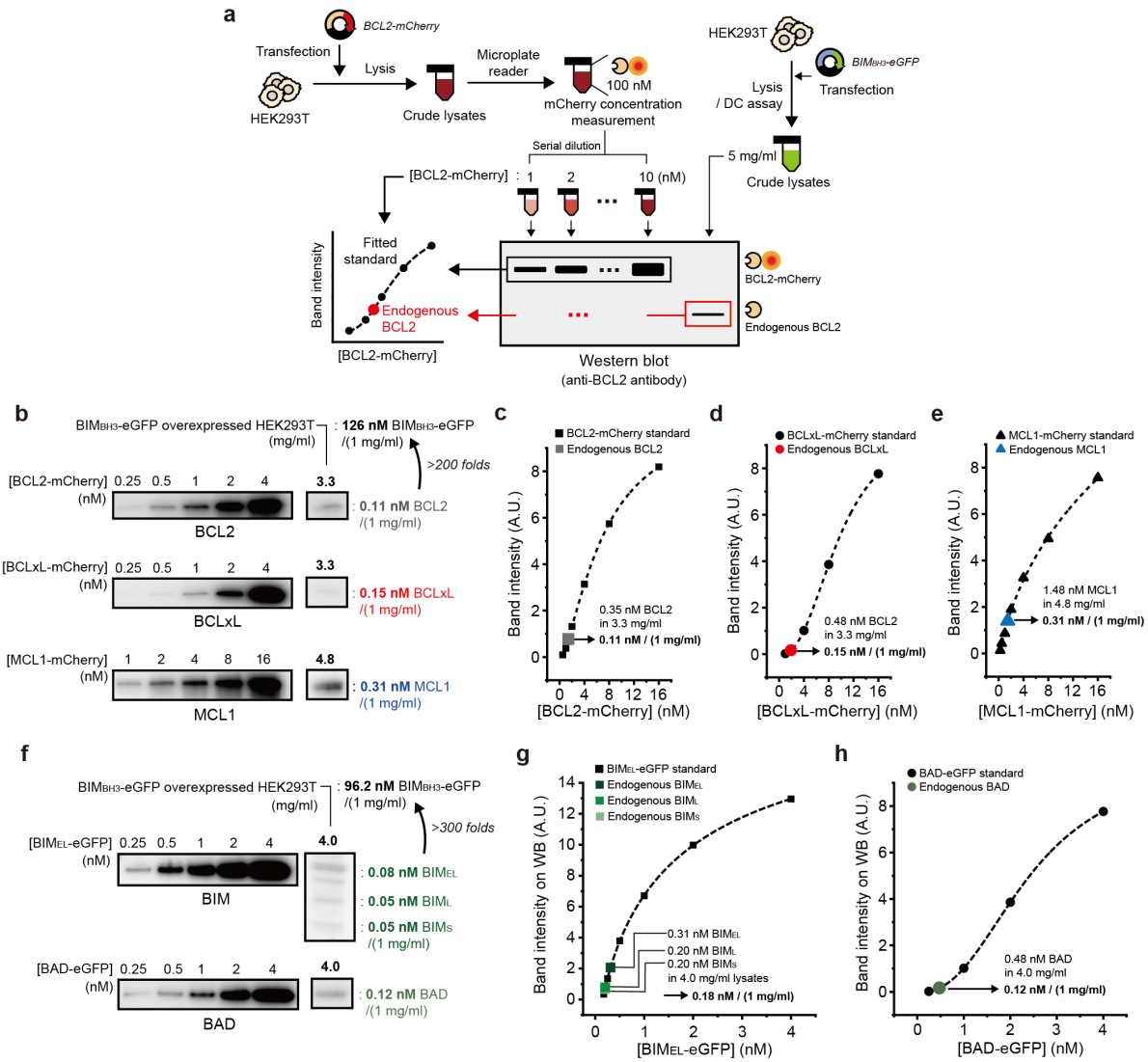

Supplementary Fig. 3: Measurement amount of endogenous BCL2 family proteins in HEK293T lysates. a, Schematic for the measurement of endogenous BCL2 family proteins using western blot. mCherry-labeled BCL2 was overexpressed in HEK293T, and BCL2-mCherry concentration in crude cell lysates was quantified with a microplate reader. The lysates were serially diluted according to the mCherry concentration and loaded to the blot. The blot was detected with anti-BCL2 antibody, and the standard curve was fitted using the band intensity and the concentration of BCL2-mCherry. On the same blot, BIM_{BH3}-eGFP overexpressed HEK293T cell lysates were loaded, and the level of endogenous BCL2 was estimated from the standard curve. **b**, The concentration of endogenous anti-apoptotic BCL2

family proteins (BCL2, BCLxL, and MCL1) in HEK293T cell lysates after BIM_{BH3}-eGFP overexpression. **c-e**, Fitted standard curves to estimate the concentration of endogenous anti-apoptotic proteins in (b). (c) BCL2, (d) BCLxL, and (e) MCL1. **f**, The concentration of endogenous BH3-only proteins (BIM and BAD) in HEK293T cell lysates after BIM_{BH3}-eGFP overexpression. **g, h**, Fitted standard curves to estimate the concentration of endogenous BH3-only proteins in (f). (g) BIM variants (BIM_{EL}, BIM_{L}, and BIM_{S}), (h) BAD.

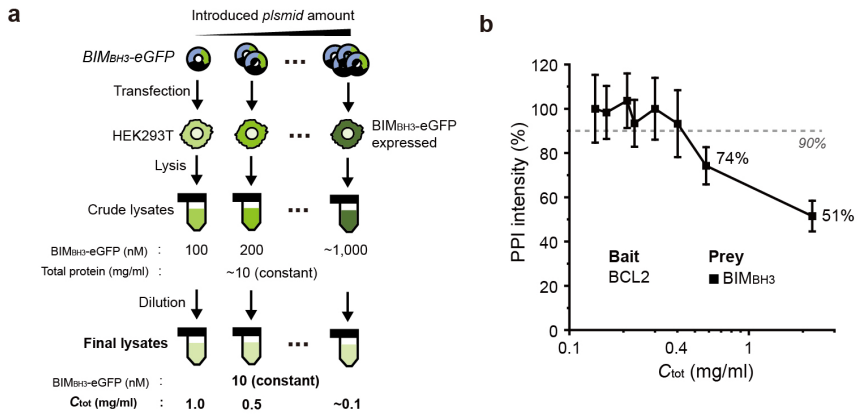

Supplementary Fig. 4: Changes in PPI of BIM$_{BH3}$-eGFP prey according to the expression rate. a, Schematic for the expression of BIM$_{BH3}$-eGFP with different C_{tot} values at the cellular level. **b**, Relative change in BCL2-BIM$_{BH3}$ PPI intensity according to the increase of C_{tot}. All data are normalized to the lowest C_{tot} sample in each experiment.

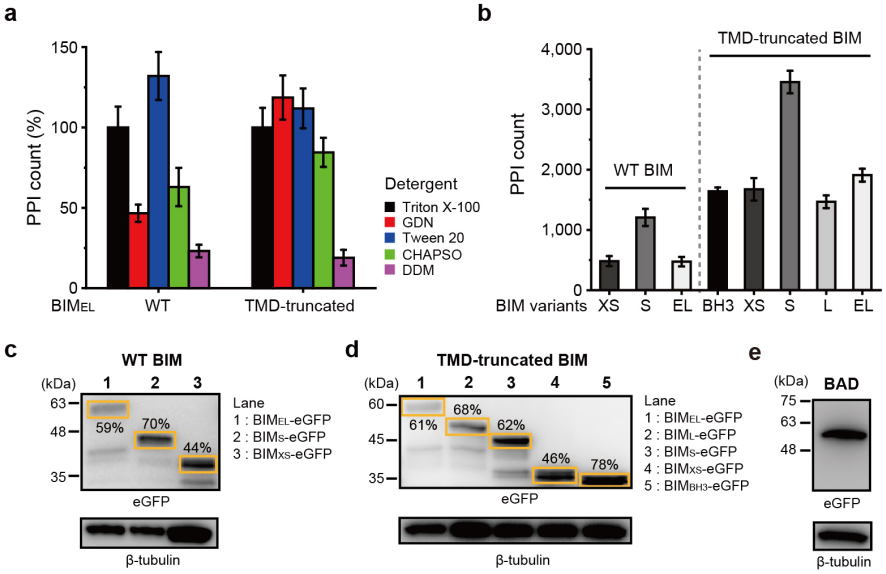

Supplementary Fig. 5: The transmembrane domain of BIM was delicately affected to the detergent condition for PPI. a, Normalized relative changes in PPI counts of WT BIM_{EL} and TMD-truncated BIM_{EL} for BCL2 with various detergent conditions in the reaction buffer. The concentration of detergent in the reaction buffer was all maintained at 0.03%. All data are normalized to Triton X-100 conditions in each experiment. **b**, PPI counts of 10 nM BIM variants for BCL2 in Triton X-100 condition. **c, d**, Expression of splicing variants of BIM proteins in HEK293T. (c) WT BIM (BIM_{EL}, BIM_S, and BIM_{XS}), (d) TMD-truncated BIM (BIM_{EL}, BIM_L, BIM_S, BIM_{XS}, and BIM_{BH3}). **e**, Expression of BAD-eGFP in HEK293T. 10 ug of crude cell lysates were loaded, and BH3-only proteins were detected by biotinylated anti-GFP antibody. The band of the target protein and sporadic cleavage rate were indicated on blot images (c-e).

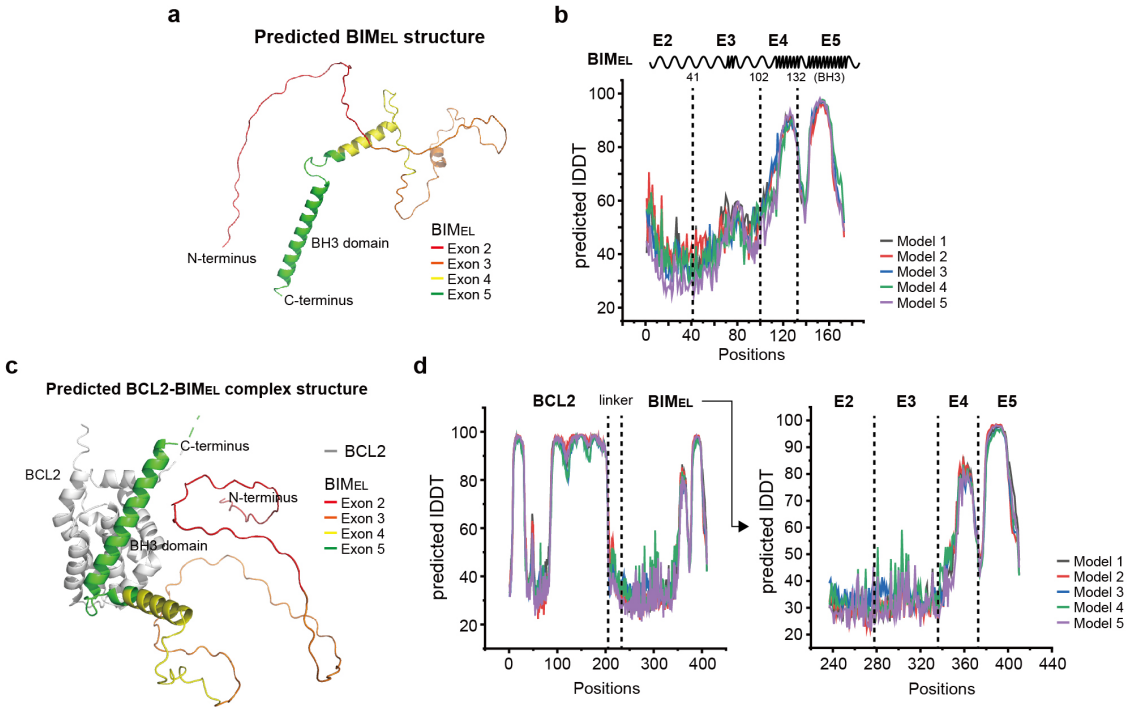

Supplementary Fig. 6: Prediction of BIM$_{EL}$ and BCL2-BIM$_{EL}$ complex structure by AlphaFold2. a, Predicted structure of BIM$_{EL}$. **b**, Predicted the local Distance Difference Test (lDDT) scores of top five BIM$_{EL}$ structure models. The spring-like figure depicts the part with the α-helix structure, and the rest for intrinsically disordered regions. **c**, Predicted structure of BCL2-BIM$_{EL}$ complex. **d**, Predicted lDDT scores of top five BCL2-BIM$_{EL}$ complex structure models. The right graph displays scores of BIM$_{EL}$ positions only. TMD sequences of BCL2 and BIM were removed for prediction (a-d). The $(GGSG)_4$ linker was inserted between the C-terminus of BCL2 and the N-terminus of BIM$_{EL}$ for complex structure prediction (c, d).

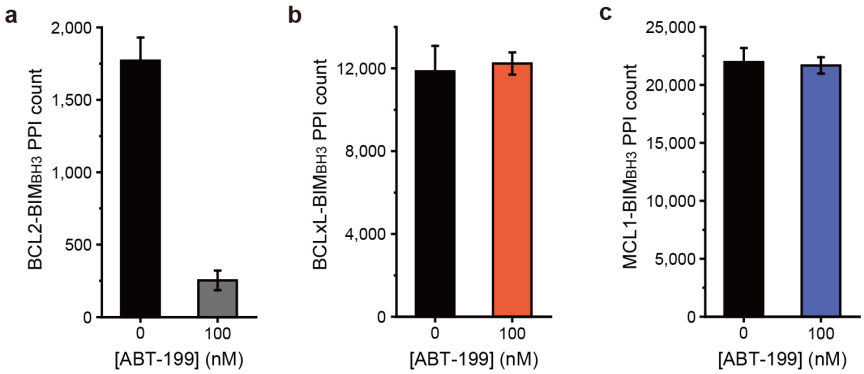

75

76 **Supplementary Fig. 7: ABT-199 selectively inhibited BCL2-BIM$_{BH3}$ PPI. a-c**, *In vitro*
77 competition of ABT-199 for PPI between different surface baits (BCL2, BCLxL, or MCL1)
78 and 10 nM of BIM$_{BH3}$-eGFP preys. ABT-199 was mixed with BIM$_{BH3}$-eGFP lysates before
79 PPI reaction (a) BCL2-BIM$_{BH3}$ PPI, (b) BCLxL-BIM$_{BH3}$ PPI, and (c) MCL1-BIM$_{BH3}$ PPI.

80

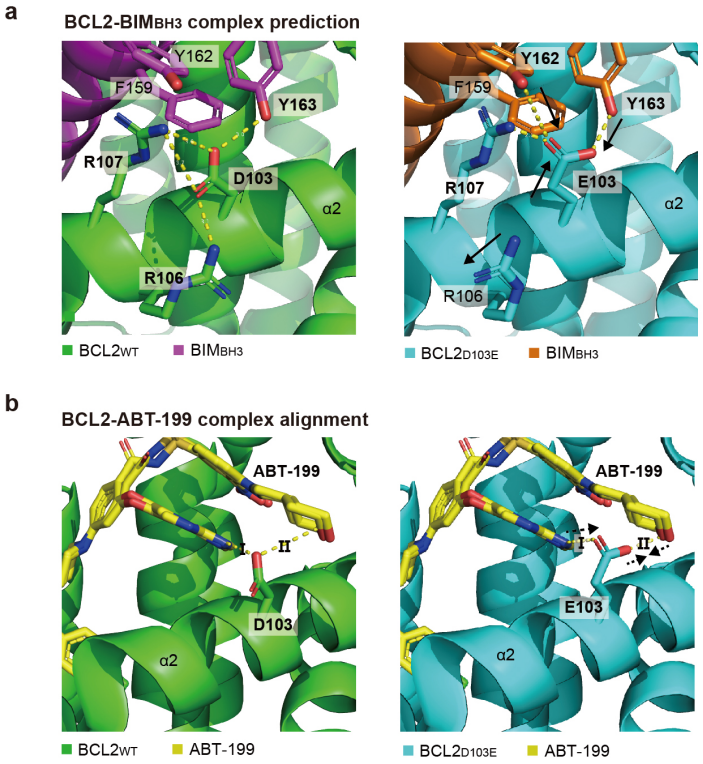

Supplementary Fig. 8: *In silico* analysis of BCL2$_{D103E}$ complex structures with BIM and ABT-199 by AlphaFold2. a, Comparison of the predicted structure of BCL2$_{WT}$-BIM$_{BH3}$ and BCL2$_{D103E}$-BIM$_{BH3}$ complexes. In E103, the negatively charged side chain is truncated in the opposite direction of WT (D103). The yellow dotted line indicates the interaction within 4Å, and the black arrow indicates the direction in which the interaction with each side chain changes after mutation (D103E). **b**, Comparison of the predicted structure of BCL2$_{WT}$-ABT-199 and BCL2$_{D103E}$-ABT-199 complexes. The BCL2-BIM$_{BH3}$ complex predicted in (a) and the known BCL2$_{G101V}$-ABT-199 structure (PDB id: 6O0k)[35] were aligned for comparison. The ABT-199 conformers are indicated in yellow. Interaction I refers to the electrostatic interaction between the indol-ring of ABT-199 and the side chain of D103 residue on BCL2. Interaction II refers to the hindrance between ABT-199 and D103 residue. E103 shows weaker electrostatic interaction for interaction I, and stronger hindrance for interaction II.

Bait	Prey	K_d (nM, n = 3)	Mean	s.d.	CV (%)
BCL2 WT	BIM_{BH3}	50.2	50.0	1.25	**2.51**
		51.2			
		48.7			
BCL2 WT	BIM_{XS}	45.6	47.2	3.82	**8.08**
		44.5			
		51.6			
BCL2 WT	BIM_{S}	17.8	18.5	0.84	**4.55**
		18.3			
		19.4			
BCL2 WT	BIM_{L}	62.8	64.6	5.72	**8.85**
		60.0			
		71.0			
BCL2 WT	BIM_{EL}	25.3	27.8	2.44	**8.78**
		30.1			
		28.1			

intra-assay CV = 6.55 (%)

Supplementary Table 1: Fitted K_d of BIM variants for BCL2 to evaluate intra-assay CV. All the K_d data are shown for each independent experiment. CV for each PPI pair was calculated by CV= s.d./mean (%) for three technically independent replicates. The intra-assay CV is the average of five CV values from each PPI pair.

Bait	Prey	BCL2 K_d (nM ± error, n = 3)	95% CI
BCL2 WT	BIM_{BH3}	**53.6** ± 1.4	(50.9 - 56.3)
BCL2 G101V	BIM_{BH3}	**98.5** ± 2.1	(94.4 - 102.6)
BCL2 D103E	BIM_{BH3}	**32.1** ± 0.7	(30.7 - 33.5)
BCL2 WT	BIM_{EL}	**27.3** ± 2.0	(23.4 - 31.2)
BCL2 G101V	BIM_{EL}	**86.6** ± 1.7	(83.3 - 89.9)
BCL2 D103E	BIM_{EL}	**34.6** ± 1.5	(31.7 - 37.5)
BCL2 WT	BAD	**3.6** ± 0.2	(3.2 - 4.0)
BCL2 G101V	BAD	**22.3** ± 1.0	(20.3 - 24.3)
BCL2 D103E	BAD	**2.0** ± 0.1	(1.8 - 2.2)

Supplementary Table 2: Fitted K_d and 95% confidence interval (CI) of BH3-only proteins for BCL2 mutants. The fitted K_d of BH3-only proteins (BIM_{BH3}, BIM_{EL}, and BAD) for BCL2 mutants (WT, G101V, and D103E). All the K_d data shown were fitted by averages of three technically independent replicates.

Bait	Prey	K_d (nM, n = 3)	Mean	s.d.	CV (%)
BCL2 WT	BIM_{BH3}	50.2	50.0	1.25	**2.51**
		51.2			
		48.7			
BCL2 G101V	BIM_{BH3}	81.7	89.3	9.06	**10.14**
		87.0			
		99.4			
BCL2 D103E	BIM_{BH3}	27.6	30.0	2.75	**9.18**
		33.0			
		29.4			
BCL2 WT	BIM_{EL}	25.3	27.8	2.44	**8.78**
		30.1			
		28.1			
BCL2 G101V	BIM_{EL}	87.4	90.4	2.86	**3.16**
		93.0			
		90.8			
BCL2 D103E	BIM_{EL}	30.5	34.2	3.28	**9.59**
		36.7			
		35.5			
BCL2 WT	BAD	4.0	3.7	0.30	**8.20**
		3.6			
		3.5			
BCL2 G101V	BAD	20.0	22.7	2.43	**10.71**
		24.7			
		23.4			
BCL2 D103E	BAD	1.8	2.2	0.35	**15.99**
		2.2			
		2.5			

intra-assay CV = 8.70 (%)

Supplementary Table 3: Fitted K_d of BH3-only proteins for BCL2 mutants to evaluate intra-assay CV. The fitted K_d of BH3-only proteins (BIM_{BH3}, BIM_{EL}, and BAD) for BCL2 mutants (WT, G101V, and D103E). All the K_d data are shown for each independent experiment. CV for each PPI pair was calculated by CV= s.d./mean (%) for three technically independent replicates. The intra-assay CV is the average of five CV values from each PPI pair.

Purpose of primers	Primer sequence (5' to 3')	
(*BCL2 mutation*)		
BCL2 G101V mutation	F	cgc cag gcc gtc gac gac tt
	R	aa gtc gtc gac ggc ctg gcg
BCL2 D103E mutation	F	gcc ggc gac gaa ttc tcc cg
	R	cg gga gaa ttc gtc gcc ggc
(*BIM splicing variants*)		
BIMS isolation	F	cc cta cag aca gag cca caa gct tcc atg agg cag gct
	R	tc agc ctg cct cat gga agc ttg tgg ctc tgt ctg tag
BIMXS isolation	F	gt ccg aag cgc gcg gaa ttc atg agg cag gct gaa cct
	R	cc cgt cga ctg cag aat tct atg cat tct cca cac cag
(*TMD-truncated BIM splicing variants*)		
BIMEL isolation	F	cg agc tca agc ttc gaa ttc atg gca aag caa cct tct
	R	cc cgt cga ctg cag aat tct ttg gta att att caa aaa
BIML isolation	F	ag cca caa gac agg agc cca gca ccc
	R	ct cct gtc ttg tgg ctc tgt ctg tag gga gg
BIMS isolation	F	gag cca caa gct tcc atg agg cag gct g
	R	at gga agc ttg tgg ctc tgt ctg tag gga gg
BIMXS isolation	F	c ttc gaa ttc atg agg cag gct gaa cct g
	R	ctg cct cat gaa ttc gaa gct tga gct cga gat c
BIMBH3 isolation	F	cg agc tca agc ttc gaa ttc atg agg cag gct gaa cct
	R	ac cgt cga ctg cag aat tcc cct cct tgc ata gta agc

Supplementary Table 4: Sequences of used oligonucleotide primers (F: forward primer, R: reverse primer).